Revealing the Emergence of Classicality Using Nitrogen-Vacancy Centers

T. K. Unden,[1] D. Louzon,[1,2] M. Zwolak,[3] W. H. Zurek,[4] and F. Jelezko[1,5]
[1]*Institute for Quantum Optics, Ulm University, Albert-Einstein-Allee 11, Ulm 89081, Germany*
[2]*Racah Institute of Physics, The Hebrew University of Jerusalem, Jerusalem 91904, Israel*
[3]*Biophysics Group, Microsystems and Nanotechnology Division, Physical Measurement Laboratory, National Institute of Standards and Technology, Gaithersburg, Maryland 20899, USA*
[4]*Theory Division, Los Alamos National Laboratory, Los Alamos, New Mexico 87545, USA*
[5]*Center for Integrated Quantum Science and Technology (IQ^{st}), Ulm University, Ulm 89081 Germany*

(Received 8 March 2019; revised manuscript received 8 August 2019; published 1 October 2019)

The origin of classical reality in our quantum world is a long-standing mystery. Here, we examine a nitrogen-vacancy center in diamond evolving in the presence of its magnetic nuclear spin environment which is formed by the natural appearance of carbon ^{13}C atoms in the diamond lattice, to study quantum Darwinism—the proliferation of information about preferred quantum states throughout the world via the environment. This redundantly imprinted information accounts for the perception of objective reality, as it is independently accessible by many without perturbing the system of interest. To observe this process, we implement a novel dynamical decoupling scheme that enables the measurement and control of several nuclear spins (the environment $\mathcal{E}$) interacting with a nitrogen vacancy (the system $\mathcal{S}$). Our experiment demonstrates that, in the course of the decoherence of $\mathcal{S}$, redundant information is indeed imprinted onto $\mathcal{E}$, giving rise to incipient classical objectivity—a consensus recorded in redundant copies, and available from the fragments of the nuclear spin environment $\mathcal{E}$, about the state of $\mathcal{S}$. This provides the first laboratory verification of the process responsible for the emergence of the objective classical world from the underlying quantum substrate.

DOI: 10.1103/PhysRevLett.123.140402

Quantum Darwinism—a theoretical framework for describing the emergence of the classical world from the quantum—recognizes that the environment is a communication channel through which observers acquire information. This upgrades the role of the environment from the one it had in decoherence theory (i.e., just suppressing quantum superpositions) and provides a framework for understanding and quantifying the emergence of the objective classical world [1–11]. In the process of decohering a system, the environment selectively acquires information about certain system states—the pointer states [12] that are resistant to decoherence—and transmits it to observers who can then find out about $\mathcal{S}$ independently and indirectly via $\mathcal{E}$. In our world the same photon environment that contributes to decoherence simultaneously and inherently gives rise to our perception of objective states of fundamentally quantum systems. These are the pointer states that survive the interaction with the environment and promulgate information about themselves into the world.

This process of selective proliferation of information responsible for the emergence of the classical world is most effective on the macroscopic level (when "order" Avogadro's number of environment components interact with the system), but it has to be studied in the microscopic quantum domain. Decohering interactions of a class that includes the photon environment, as well as spin and other models (so-called "pure decoherence"), universally give

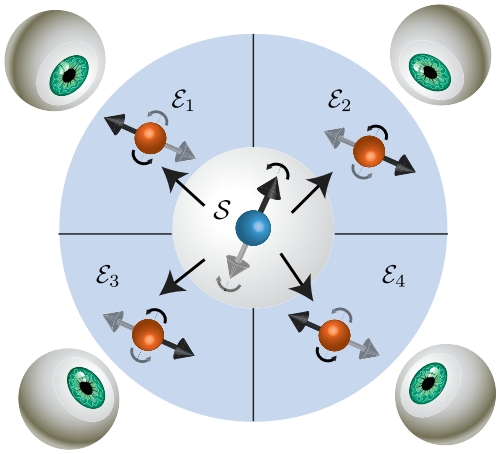

FIG. 1. The nuclear spin environment as a quantum communication channel. A central electronic spin—the system $\mathcal{S}$—is surrounded by multiple nuclear spins $\mathcal{E}_k$ comprising the environment $\mathcal{E}$. The environment spins are effectively isolated from each other due to their weak spin-spin interaction. The interaction between the central spin and an individual nuclear spin is mediated by the hyperfine interaction and depends on the relative position of each spin. The hyperfine interaction strength is therefore different for each nuclear spin. The environment decoheres the system and, in the process, each of its components is rotated into a new state (black and gray arrows) conditional on the central spin state. Multiple observers (eyes) can access different environment spins and thus independently deduce the state of the system.

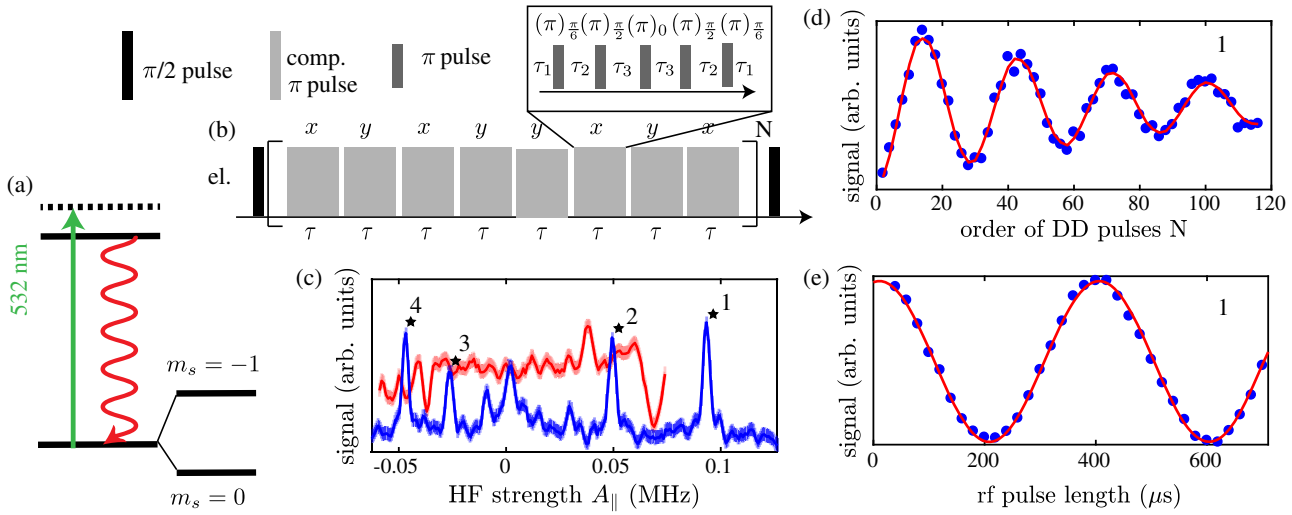

FIG. 2. Experimental control of the nuclear-electronic spin system. (a) Energy level diagram of the electronic spin of a NV center. The orbital configuration can be optically excited with green laser light and the passage through the excited state is manifested by red fluorescence. Each orbital state carries a spin triplet ($S = 1$) manifold. Spin-dependent nonradiative decay can be used for optical spin detection and efficient spin initialization of the ground state spin sublevel $|m_s = 0\rangle$. In this work we focus on the two-level-system specified by the ground state spin sublevels $|m_s = 0\rangle \equiv |\uparrow\rangle$ and $|m_s = -1\rangle \equiv |\downarrow\rangle$. (b) The adaptive $XY8^N$ sequence. The DD sequence is a train of composite π pulses with a single pulse duration of τ and an alternating orthogonal phase (here x and y) for robustness. Each composite π pulse is a symmetric sequence of five microwave π pulses (inset) with different pulse phases to achieve robustness against single pulse imperfections. (c) Measured spectrum (blue) when the interpulse spacing $\tau = 1/(\omega_L + A_\parallel/2)$ of an AXY^{16} sequence varies, where ω_L specifies the bare Larmor frequency of nuclear carbon spins determined by the external, applied magnetic field (here, ≈440 G). For comparison, the result of a standard $XY8^{16}$ spectrum is shown in red. The solid lines are smoothed data and the light-blue–red shaded regions represent one standard deviation. The four strongest coupled nuclear spins are marked by stars with corresponding numbers and the parallel hyperfine coupling strengths 93.5, 49.5, −26.3, and −47.1 kHz are identified. (d) NV spin mediated Rabi oscillations of a single nuclear spin. The interpulse spacing τ is tuned to the Larmor period of carbon spin 1 and the order N of the AXY sequence is increased. The red curve is the result of a simulation, when the measured hyperfine values (see Sec. III in the Supplemental Material [20]) are taken into account. (e) Rabi oscillation of nuclear spin 1 driven by a radio frequency (rf) field. AXY sequences are used for initialization and readout of the nuclear spin (see Sec. I in the Supplemental Material [20] for more information). The solid curve is a cosine fit corresponding to a sum of squares error of 2.4×10^{-4}. Errors are smaller than the data points in (d),(e).

rise to redundant imprinting of information which in turn gives rise to objective classical reality [7,9]. Central spin systems, in particular, offer ideal test cases to observe this emergence in action and even control it, see Fig. 1. Such experiments are still rather challenging. Real systems are inhomogeneous, which means measurement and control requires addressing disparate components. Moreover, the central system and the subsystems of the model environment tend to interact with everything and, together with spectral broadening, this makes identifying and selecting the most relevant interactions difficult. Nitrogen-vacancy (NV) centers provide an interesting setup where some of these issues can be solved, as we will show.

We will focus on the single electron spin in an NV center [13,14], Fig. 2(a), embedded in a room-temperature diamond environment that carries nuclear ^{13}C spins (with the natural abundance of 1.1%). The diamond sample is grown via chemical vapor deposition and single NV centers are introduced into the diamond from residual nitrogen in the chemical vapor deposition plasma. Such a platform—a central electron spin coupled to nuclear ancilla spins—has also been studied in previous experiments in different contexts [15–17]. In the secular approximation [18], the Hamiltonian is

$$\mathbf{H} = 2\pi S_z \sum_k A_\parallel^k I_z^k, \tag{1}$$

where $S_z = |\uparrow\rangle\langle\uparrow|$ is a shifted z operator for the electron spin, I_z^k is the spin-1/2 operator for the nuclear spin k, and $A_\parallel^k$ is the parallel component of the hyperfine interaction (HF) vector $\vec{A}^k$. This is of the pure decoherence form, where environment components interact with the system and do not interact with each other [7,9,19]. The eigenstates of S_z are the so-called pointer states of the system [12]—the states that are not perturbed by the environment even though their superpositions decohere. For an initial state where the electron spin is in a nonclassical quantum superposition, $|+\rangle = |\uparrow\rangle + |\downarrow\rangle$, and in a product state with the environment spins (individually in an initialized state $|\phi_k\rangle$),

$$|\psi(0)\rangle = |+\rangle_S \otimes \left(\bigotimes_k |\phi_k\rangle\right), \tag{2}$$

the state after evolving for a time t is

$$|\psi(t)\rangle = |\uparrow\rangle_S \otimes \left(\bigotimes_k |\phi_{k|\uparrow}\rangle\right) + |\downarrow\rangle_S \otimes \left(\bigotimes_k |\phi_{k|\downarrow}\rangle\right). \quad (3)$$

The superposition in the system has "branched out" into the environment, creating correlations with the nuclear spins via conditional rotations into the states $|\phi_{k|\hat{s}}\rangle$ with $\hat{s} = \uparrow, \downarrow$ the pointer states of the system [the $m_s = 0$ and -1 states of the NV center, respectively, see Fig. 2(a)].

When $|\phi_k\rangle = |+\rangle$, $A_\parallel^k = A_\parallel$, and $t = 1/(2A_\parallel)$, the state in Eq. (3) is a Greenberger-Horne-Zeilinger (GHZ) state, where each environment spin holds a perfect record of the pointer state; i.e., the conditional states $|\phi_{k|\uparrow}\rangle$ and $|\phi_{k|\downarrow}\rangle$ are orthogonal and thus the system's pointer state can be inferred exactly. Under more general conditions, the state is GHZ-like and each spin only holds a partial record of the system's state. In either case, the information can be quantified by the quantum mutual information between the system $\mathcal{S}$ and a fragment $\mathcal{F}$ of the environment,

$$I(\mathcal{S}:\mathcal{F}) = H_\mathcal{S}(t) + H_\mathcal{F}(t) - H_{\mathcal{SF}}(t), \quad (4)$$

where $H_\mathcal{A} = -\mathrm{tr}\rho_\mathcal{A}\log_2\rho_A$ is the von Neumann entropy of subsystem $\mathcal{A}$. This decomposes into classical and quantum components [5],

$$I(\mathcal{S}:\mathcal{F}) = \chi(\Pi_\mathcal{S}:\mathcal{F}) + \mathcal{D}(\Pi_\mathcal{S}:\mathcal{F}). \quad (5)$$

The first component is the Holevo quantity [27,28]

$$\chi(\Pi_\mathcal{S}:\mathcal{F}) = H_\mathcal{F}(t) - \sum_s p_s H_{\mathcal{F}|s}(t), \quad (6)$$

which upper bounds the classical information communicated by a quantum channel, i.e., here, information about the observable $\Pi_\mathcal{S}$ on the system $\mathcal{S}$ communicated by an environment fragment $\mathcal{F}$. The second component, $\mathcal{D}(\Pi_\mathcal{S}:\mathcal{F})$, gives the quantum discord [29–31]. The quantity $H_{\mathcal{F}|s}$ is the entropy of $\mathcal{F}$ conditioned on outcome s in $\mathcal{S}$ (with probability p_s).

In principle, one can examine the information about any observable of $\mathcal{S}$, but under decoherence it is information about the pointer states of $\mathcal{S}$, $\hat{\Pi}_\mathcal{S}$ (S_z in our case), that is imprinted on $\mathcal{F}$ [1,5]. In what follows, we will determine $\chi(\hat{\Pi}_\mathcal{S}:\mathcal{F})$ in a natural setting. We focus on the Holevo information because its complement in the equation for mutual information—quantum discord $\mathcal{D}(\hat{\Pi}_\mathcal{S}:\mathcal{F})$—describes correlations between $\mathcal{S}$ and $\mathcal{F}$ that cannot be shared by observers [32], and, hence, cannot help establish objective reality. We thus focus only on $\chi(\hat{\Pi}_\mathcal{S}:\mathcal{F})$ and will discuss possibilities for obtaining $\mathcal{D}(\hat{\Pi}_\mathcal{S}:\mathcal{F})$ afterward.

In the case of the generation of a perfect GHZ state (see artificial, experimental creation in Sec. IV of the Supplemental Material [20]), the Holevo information is 1 bit for any fragment of the environment: The original system's state is perfectly decohered and each environment spin carries a record of the system's pointer state. Thus, when several observers each independently intercept one spin from the environment, they can all find out that state independently as each can examine separate fragment of $\mathcal{E}$—individual environment spin. This is the notion of redundancy, that there are (in this ideal case) $\sharp\mathcal{E}$ copies of the information about the system in the environment of size $\sharp\mathcal{E}$. Departing from ideality, the redundancy R_δ will be $\sharp\mathcal{E}/\sharp\mathcal{F}_\delta$, where $\sharp\mathcal{F}_\delta$ is the size of the typical fragment required to obtain

$$\langle\chi(\hat{\Pi}_\mathcal{S}:\mathcal{F})\rangle \geq (1-\delta)H(\hat{\Pi}_\mathcal{S}). \quad (7)$$

That is, the fragment size, on average, to get more than $H(\hat{\Pi}_\mathcal{S})$ of the missing information about $\mathcal{S}$. The quantity δ is the information deficit—the finite precision one has to pay for the lack of ideality.

It is clear that to observe this process in the laboratory, one either has to perform full quantum state tomography or, to see that there is redundant information, address the individual nuclear spins. State-of-the-art technology uses dynamical decoupling (DD) to tackle issues such as these. However, selectivity in a spectrally dense environment is still a difficult task. Here, we implement a novel DD protocol, theoretically proposed in Refs. [33,34], to both identify the spin environment and to control individual parts of it. Like well-established DD sequences such as the Carr-Purcell-Meiboom-Gill sequence [35] or $XY8$ [36], the protocol employs repetitive central spin flips via a microwave drive, where the interpulse spacing determines the frequency of the control window. However, the new protocol, the adaptive $XY8$ ($AXY8$) sequence, establishes a robust control of individual nuclear spins mediated by the central electron spin by arbitrarily shaping the DD control filter. This refocuses undesired noise, allowing for the identification and control of individual nuclear spins.

More specifically, control of the filter design is supplied by replacing each single spin flip by a train of five pulses, see the inset of Fig. 2(b). An alternating rotation axis (phase) of the microwave pulses permits a robust operation in the presence of pulse errors. In addition, time evolution during the pulse train models an arbitrary filter response, where the evolution times τ_1, τ_2, and τ_3 are numerically calculated with a specific filter function (see Sec. I in the Supplemental Material [20]). In the case that the nuclear Zeeman energy is much larger than the hyperfine coupling strength, the process is modeled by the effective Hamiltonian [33]

$$H^k = \frac{1}{2} f_{\mathrm{DD}} A_\perp \left(S_z - \frac{1}{2}\right) I_x^k, \quad (8)$$

when the interpulse spacing τ matches the corresponding Larmor frequency of nuclear spin k. I_x^k is the corresponding

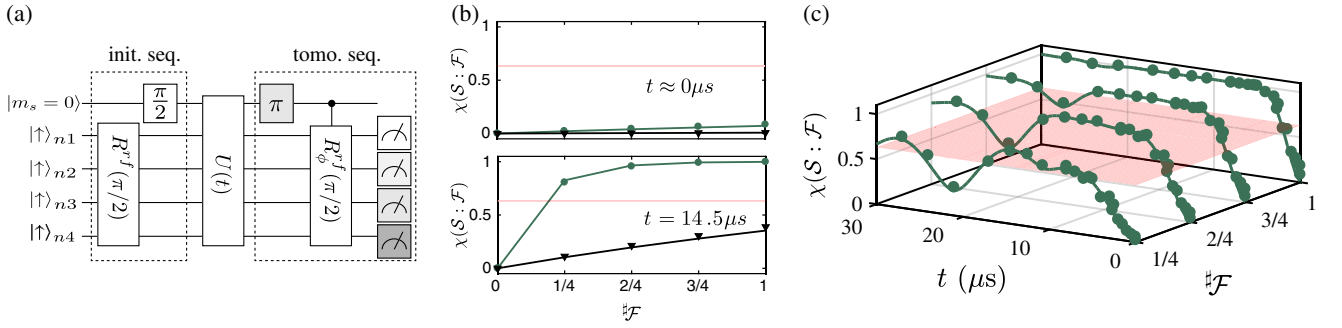

FIG. 3. The emergence of redundancy for an NV center being naturally decohered by its environment. (a) The NV spin is first initialized optically and its polarization swapped to each individual nuclear spin by a repetitive process (not shown). Two $\pi/2$ pulses transform the product state into a product state of $|+\rangle$ states. These then evolve under the direct HF interaction between the NV center and nuclear spins [$U(t)$]. Single nuclear spin tomography in the electronic subspace $|m_s=-1\rangle$ is performed by a selective $\pi/2$ pulse mediated by a weak, resonant rf pulse (R^{rf}_ϕ). In addition, multiple measurements are performed with different rf pulse phases ϕ to determine the phase of the nuclear spin superposition. An optional π pulse in front of the last rf pulse can be applied for nuclear spin tomography in the electronic $|m_s=0\rangle$ subspace. The state of a single nuclear spin is in the end swapped to the NV spin and an optical readout follows. (b) Holevo information versus fraction size for two different free evolution times. (c) Holevo information $\chi(\hat{\Pi}_S:\mathcal{F})$ versus the environment fragment size $\sharp\mathcal{F}$ and free evolution time t. The solid curves in (b) and (c) show the results of simulations with and without imperfect initial polarization. The dynamics in the simulation are governed by the Hamiltonian H_0, Eq. (1). The semitransparent red lines in (b) and the plane in (c) indicate an information deficit of $1/e$, i.e., $I=(1-1/e)H_S$. Errors are smaller than the data points.

nuclear spin-1/2 operator in the x direction and f_{DD} a variable parameter, determining the DD control filter.

The effective interaction strength $f_{\mathrm{DD}}\mathcal{A}_\perp/2$ is mediated by the perpendicular HF coupling $A_\perp$, which is here determined by the magnetic dipole-dipole interaction. Instead of a constant interaction strength, determined by $A_\perp$, a weaker effective strength can be modeled without the necessity of using higher harmonics [18,37], which are more vulnerable to pulse error, to achieve individual nuclear spin addressing. Further experiments (see Sec. I of the Supplemental Material [20]) performed with different filter coefficients confirm the concept of the AXY sequence and artifacts coming from contributions of higher harmonics can be neglected due to a large detuning. An AXY spectrum (with $f_{\mathrm{DD}}=0.2$) of the nuclear spin environment is shown in Fig. 2(c) (blue curve). Because of electron-nuclear spin entanglement governed by Eq. (8), four stronger coupled nuclear spins and additional, more weakly coupled ones can be identified by their different parallel HF interaction strength, when the interpulse spacing τ varies. The effective coupling strength was here reduced by about a factor of 5 compared to the dipolar HF interaction strength determined by the register geometry. The result of the typical, nonadaptive $XY8$ sequence (red curve) does not show the features. The HF interaction strength is too strong, and therefore the resonances too broad to identify individual spins. The rising and falling of quantum correlations between the electronic spin and a nuclear spin is shown in Fig. 2(d), when the repetition N of the pulse sequence is increased, while the pulse spacing is kept constant and on resonance with the Larmor period of nuclear spin one. In addition, the result in Fig. 2(e) shows a Rabi oscillation of nuclear spin one induced by a resonant rf field, when a iSwap gate [34] based on the AXY sequence is used for nuclear spin initialization and readout (see more information in Sec. I of the Supplemental Material [20]).

In previous work, redundancy was created artificially via the construction of a GHZ state, which was achieved for example recently with photonic simulators [38,39]. In addition, work in the field of quantum nondemolition measurements [40–43] were also able to create highly redundant states by consecutive two-body scattering. However, in our everyday world, redundancy appears as a consequence of natural interactions between an $\mathcal{S}$ and $\mathcal{E}$ initially out of equilibrium. To observe this in NV centers, we allow in the following the system to evolve freely in the presence of the natural HF interaction. Because the effect of the nuclear spin environment on the central electron spin is dominated by the nuclear spins close to the central spin, we concentrate on the four strongest coupled nuclear spins [see Fig. 2(c)]. The experimental protocol is shown in Fig. 3(a). We first initialize the system into the out-of-equilibrium product state, Eq. (2), with $|\phi_k\rangle=|+\rangle$. This is followed by the free evolution of $\mathcal{SE}$ of duration t according to the HF Hamiltonian, Eq. (1). To determine the classical correlations of fragments $\mathcal{F}$ of the environment with $\mathcal{S}$, tomography is applied by an electron spin-selective nuclear rf pulse with variable phase ϕ, which rotates only an individual nuclear spin (see Secs. II and IV in the Supplemental Material [20] for more information). Nuclear spin initialization and readout is achieved by a nuclear spin-selective iSwap gate mediated by the AXY sequence.

Figure 3(b) shows the Holevo information versus fraction size for two different evolution times and Fig. 3(c)

shows the full data set. When errors happen during the nuclear spin polarization as well as tomography, and both sorts of errors are corrected in the analysis (see Sec. II of the Supplemental Material [20]), the results are shown in dark green. When only the errors of an imperfect tomography are corrected in the analysis, the data are presented in black. Here, we focus on the dark green data set. At short times, there is essentially no information in fragments or even the whole environment, as initially the $\mathcal{SE}$ state is a product state. As time develops, however, information is rapidly transferred into the environment. At a time of 14.5 μs even a single nuclear spin captures nearly complete information, to within an information deficit of $1/e$ bits. In other words, all the four most strongly coupled nuclear spins have nearly a complete record of the system's pointer state. This redundancy is reflected in the presence of a plateau in the Holevo information versus fragment size. We note also that the timescale of information rising (on the order of several μs) is in good agreement with the NV spin coherence time measured by a Ramsey experiment, see Sec. VII in the Supplemental Material [20]. With increasing time, though, small fragments will see information flow back into the system. This is due to the fact that for individual spins the conditional states first get rotated away from each other and then back towards each other. How fast this conditional rotation of an individual nuclear spin will take place is mediated by the HF coupling. For example, the observed decrease in the Holevo information at a time of about 20 μs is due the conditional rotations of nuclear spin one, two, and four which fulfill almost 2π cycles. For a sufficiently large number of spins with random interaction strengths, even this information flow into a single spin will be one way on average. For larger fragment sizes, the information tends more and more to be one way, although there will still be periods of recurrence for long enough waiting times. When the experimental data are not normalized with respect to the initial degree of polarization (black data), redundancy is suppressed due to the lower—but nonzero except for cases of measure zero [7,9]—information capacity of the "hazy" environmental fragments [44,45].

We have exhibited the emergence of redundancy under decoherence using NV centers. Our study also provides insights into the reason for the selective banishing of quantum information: the initial superposition becomes encoded into the inaccessible global quantum correlations. This global coherence leaves a signature in the quantum mutual information [$\mathcal{D}(\hat{\Pi}_{\mathcal{S}}:\mathcal{F})$, the counterpart to $\chi(\hat{\Pi}_{\mathcal{S}}:\mathcal{F})$ in Eq. (5)] in the form of an "uptick"—a sharp upward turn of the mutual information on the plateau when the fragment size nears the total environment size [5]. This can be observed artificially, e.g., in isolated photonic simulators [38,39] and similar settings where couplings between $\mathcal{S}$ and elements of $\mathcal{E}$ are artificially controlled. Within natural settings, though, interactions with inaccessible environment components, as well as imperfect readout or initialization of the accessible environment components, make observing the uptick very challenging. Indeed, the inaccessibility of the uptick due to the interactions with many environment components is what makes our everyday world classical [5]. Thus, it is no surprise that it is difficult to measure in naturally decohering systems. Further refinement of the DD technique and samples, together with low temperature measurements, may make this uptick accessible. This will motivate future experiments in NV centers embedded in moderately ^{13}C enriched diamond (see Sec. VIII in the Supplemental Material [20]) to observe large amounts of redundancy.

Our results provide the first laboratory demonstration of quantum Darwinism in action in a natural environment. This demonstration required implementing a novel DD protocol. The process by which nuclear spin decoherence of NV centers gives rise to incipient classical objectivity is analogous to the one that occurs when photons scatter from objects in our macroscopic world. In both cases, flagrantly nonclassical (e.g., nonlocal) quantum superpositions are embedded in the larger environment, initially out of equilibrium. Interactions with the environment select certain preferred (pointer) states of the system, decohering their superpositions and proliferating accessible information about such einselected states into the world, thus relegating nonredundant quantum correlations to inaccessible regions of the Hilbert space. Our work shows that already on the atomic scale there is evidence of the process that—in everyday settings, and for much larger environments—leads to the emergence of classicality. The appearance of objective, classical states accessible to indirect measurements is anticipated by processes that take place already in small environments, and it simply gets more difficult to avoid classicality as the environment size grows. This straightforward and purely quantum account of the origins of the classical in our quantum Universe suggests other approaches to the quantum-to-classical transition (gravitational collapse, etc.) are not necessary to describe the emergence of our objective, classical world.

We thank Jorge Casanova, Zhenyu Wang, Liam P. McGuinness, and C. Jess Riedel for helpful discussions. This work was supported by the DOE LDRD program at Los Alamos National Laboratory, FQX, ERC, VW Stiftung, BW Stiftung, DFG, and BMBF. W. H. Z. acknowledges partial support by the Foundational Questions Institute Grant No. FQXi-1821, and Franklin Fetzer Fund, a donor advised fund of the Silicon Valley Community Foundation.

[1] H. Ollivier, D. Poulin, and W. H. Zurek, Phys. Rev. Lett. **93**, 220401 (2004).

[2] H. Ollivier, D. Poulin, and W. H. Zurek, Phys. Rev. A **72**, 042113 (2005).

[3] R. Blume-Kohout and W. H. Zurek, Found. Phys. **35**, 1857 (2005).
[4] W. H. Zurek, Nat. Phys. **5**, 181 (2009).
[5] M. Zwolak and W. H. Zurek, Sci. Rep. **3**, 1729 (2013).
[6] W. H. Zurek, Phys. Today **67**, No. 10, 44 (2014).
[7] M. Zwolak, C. J. Riedel, and W. H. Zurek, Phys. Rev. Lett. **112**, 140406 (2014).
[8] F. G. S. L. Brandão, M. Piani, and P. Horodecki, Nat. Commun. **6**, 7908 (2015).
[9] M. Zwolak, C. J. Riedel, and W. H. Zurek, Sci. Rep. **6**, 25277 (2016).
[10] M. Zwolak and W. H. Zurek, Phys. Rev. A **95**, 030101(R) (2017).
[11] P. A. Knott, T. Tufarelli, M. Piani, and G. Adesso, Phys. Rev. Lett. **121**, 160401 (2018)..
[12] W. H. Zurek, Phys. Rev. D **24**, 1516 (1981).
[13] M. W. Doherty, N. B. Manson, P. Delaney, F. Jelezko, J. Wrachtrup, and L. C. Hollenberg, Phys. Rep. **528**, 1 (2013).
[14] F. Jelezko and J. Wrachtrup, Phys. Status Solidi A **203**, 3207 (2006).
[15] T. H. Taminiau, J. Cramer, T. van der Sar, V. V. Dobrovitski, and R. Hanson, Nat. Nanotechnol. **9**, 171 (2014).
[16] M. Hirose and P. Cappellaro, Nature (London) **532**, 77 (2016).
[17] S. Zaiser, T. Rendler, I. Jakobi, T. Wolf, S.-Y. Lee, S. Wagner, V. Bergholm, T. Schulte-Herbrüggen, P. Neumann, and J. Wrachtrup, Nat. Commun. **7**, 12279 (2016).
[18] L. Childress, M. V. Gurudev Dutt, J. M. Taylor, A. S. Zibrov, F. Jelezko, J. Wrachtrup, P. R. Hemmer, and M. D. Lukin, Science **314**, 281 (2006).
[19] C. J. Riedel, W. H. Zurek, and M. Zwolak, New J. Phys. **14**, 083010 (2012).
[20] See Supplemental Material at http://link.aps.org/supplemental/10.1103/PhysRevLett.123.140402 for more information, which includes Refs. [21–26].
[21] A. M. Souza, G. A. Álvarez, and D. Suter, Phil. Trans. R. Soc. A **370**, 4748 (2012).
[22] A. Laraoui, D. Pagliero, and C. A. Meriles, Phys. Rev. B **91**, 205410 (2015).
[23] J. Baum, M. Munowitz, A. N. Garroway, and A. Pines, J. Chem. Phys. **83**, 2015 (1985).
[24] M. Gärttner, J. G. Bohnet, A. Safavi-Naini, M. L. Wall, J. J. Bollinger, and A. M. Rey, Nat. Phys. **13**, 781 (2017).
[25] K. M. R. Audenaert, J. Calsamiglia, R. Muñoz-Tapia, E. Bagan, L. Masanes, A. Acin, and F. Verstraete, Phys. Rev. Lett. **98**, 160501 (2007).
[26] A. P. Nizovtsev, S. Y. Kilin, A. L. Pushkarchuk, V. A. Pushkarchuk, S. A. Kuten, O. A. Zhikol, S. Schmitt, T. Unden, and F. Jelezko, New J. Phys. **20**, 023022 (2018).
[27] A. S. Holevo, Probl. Inf. Transm. **9**, 177 (1973).
[28] M. A. Nielsen and I. L. Chuang, *Quantum Computation and Quantum Information: 10th Anniversary Edition* (Cambridge University Press, New York, 2011), p. 531.
[29] W. H. Zurek, Ann. Phys. (Leipzig) **9**, 855 (2000).
[30] H. Ollivier and W. H. Zurek, Phys. Rev. Lett. **88**, 017901 (2001).
[31] L. Henderson and V. Vedral, J. Phys. A **34**, 6899 (2001).
[32] A. Streltsov and W. H. Zurek, Phys. Rev. Lett. **111**, 040401 (2013).
[33] J. Casanova, Z.-Y. Wang, J. F. Haase, and M. B. Plenio, Phys. Rev. A **92**, 042304 (2015).
[34] J. Casanova, Z.-Y. Wang, and M. B. Plenio, Phys. Rev. A **96**, 032314 (2017).
[35] A. Maudsley, J. Magn. Res. **69**, 488 (1986).
[36] T. Gullion, D. B. Baker, and M. S. Conradi, J. Magn. Reson. **89**, 479 (1990).
[37] T. H. Taminiau, J. Cramer, T. van der Sar, V. V. Dobrovitski, and R. Hanson, Nat. Nanotechnol. **9**, 171 (2014).
[38] M. A. Ciampini, G. Pinna, P. Mataloni, and M. Paternostro, Phys. Rev. A **98**, 020101(R) (2018).
[39] M.-C. Chen, H.-S. Zhong, Y. Li, D. Wu, X.-L. Wang, L. Li, N.-L. Liu, C.-Y. Lu, and J.-W. Pan, Sci. Bull. **64**, 580 (2019).
[40] G. Nogues, A. Rauschenbeutel, S. Osnaghi, M. Brune, J. M. Raimond, and S. Haroche, Nature (London) **400**, 239 (1999).
[41] S. Gleyzes, S. Kuhr, C. Guerlin, J. Bernu, S. Deléglise, U. Busk Hoff, M. Brune, J.-M. Raimond, and S. Haroche, Nature (London) **446**, 297 (2007).
[42] A. Lupascu, S. Saito, T. Picot, P. C. de Groot, C. J. P. M. Harmans, and J. E. Mooij, Nat. Phys. **3**, 119 (2007).
[43] P. Neumann, J. Beck, M. Steiner, F. Rempp, H. Fedder, P. R. Hemmer, J. Wrachtrup, and F. Jelezko, Science **329**, 542 (2010).
[44] M. Zwolak, H. T. Quan, and W. H. Zurek, Phys. Rev. Lett. **103**, 110402 (2009).
[45] M. Zwolak, H. T. Quan, and W. H. Zurek, Phys. Rev. A **81**, 062110 (2010).